Fluid Phase Equilibria 391 (2015) 54–66

Contents lists available at ScienceDirect

Fluid Phase Equilibria

journal homepage: www.elsevier.com/locate/fluid

# A study on the effect of ternary interaction parameters on the equation of state description of ternary fluid phase equilibria

G.O. Pisoni [a], S.B. Rodriguez-Reartes [a], J.I. Ramello [a,b], M. Cismondi [b], M.S. Zabaloy [a,*]

[a] Departamento de Ingeniería Química, Universidad Nacional del Sur Planta Piloto de Ingeniería Química, CONICET, CC 717, 8000 Bahía Blanca, Argentina
[b] Facultad de Ciencias Exactas Físicas y Naturales, Universidad Nacional de Córdoba, Av. Vélez Sarsfield 1611, Ciudad Universitaria, X5016GCA Córdoba, Argentina

ARTICLE INFO

*Article history:*
Received 3 October 2014
Received in revised form 13 January 2015
Accepted 14 January 2015
Available online 23 January 2015

*Keywords:*
High pressure
Ternary systems
Ternary interaction parameters
Phase equilibria
Equation of state
Cubic mixing rules

ABSTRACT

Models of the equation of state (EOS) type, used for describing fluid phase equilibria, typically assume that the system behavior can be described from binary contributions only. This is not enough for obtaining good predictions for the high-pressure phase equilibria of ternary highly non ideal systems. On the other hand, cubic mixing rules (CMRs) provide both, binary and ternary interaction parameters. Such ternary parameters have the potential of improving the reproduction of ternary experimental data while leaving invariant the description of the three constituent binary subsystems. In this work, we evaluate the possibilities of the CMRs approach for ternary systems by studying the phase equilibria of two of them, i.e., $CO_2$ + *n*-hexadecane + 1,8-octanediol and $CO_2$ + $H_2O$ + 2-propanol. For the system $CO_2$ + *n*-hexadecane + 1,8-octanediol, we have available both, experimental isothermal binary and ternary phase equilibrium data. For such system, we investigate the influence of the ternary parameters on the size of ternary two-phase and three-phase equilibrium regions, and compare it to that of the experimental data. We also consider predicted values of the ternary parameters, which we need when ternary experimental data are not available. For the system $CO_2$ + $H_2O$ + 2-propanol, we examine the effect of the ternary interaction parameters on some calculated ternary univariant lines, ternary invariant points and ternary three-phase equilibria, over wide ranges of conditions.

In this study, we use the Peng–Robinson (PR) EOS and Soave–Redlich–Kwong (SRK) EOS, both coupled to CMRs. Our results make evident the flexibility and improvement that can be gained in the description of ternary phase equilibria by resorting to ternary interaction parameters.



## 1. Introduction

Models of the equation of state (EOS) type are customary used to describe the phase equilibria of mixtures in liquid, vapor and supercritical states, over wide ranges of conditions. These models typically assume that the system behavior can be described from binary contributions only. Conventionally, the binary interaction parameters of the model are fit from binary fluid phase equilibrium data. Once this is done, all the predicted ternary and higher equilibria become determined by both, the pure compound parameters and the previously fit binary interaction parameters. It is well documented in the literature that the high-pressure phase equilibria of ternary highly non ideal systems is not well predicted from binary contributions [1]. More specifically, in Ref. [1], among other tests, binary interaction parameters are fit from both, binary and ternary data, simultaneously, which implies a poorer description of the binary data for the sake of improving the reproduction of the ternary experimental information [1]. It is clear that we need more flexible models. One possibility is to couple the EOS model to mixing rules written as triple summations of terms which depend on the product of three mole fractions. These are cubic mixing rules (CMRs) [2]. CMRs depend on three-index binary interaction parameters and on three-index ternary interaction parameters. For a given binary system, CMRs provide four independent interaction parameters [2]. Thus, highly asymmetric binary systems can be represented more accurately by CMRs than by quadratic mixing rules (QMRs).

Cismondi et al. [3] described the phase behavior of $CO_2$ + *n*-alkane systems in the carbon number range from 14 to 22, using the RK-PR [4] EoS coupled to temperature dependent CMRs. They [3] optimized the CMRs parameters paying attention to a number of experimental phase equilibrium key points (e.g., critical endpoints) of the binary fluid phase equilibrium characteristic

* Corresponding author. Tel.: +54 291 486 1700x232; fax: +54 291 486 1600.
*E-mail addresses:* marcelo.santiago.zabaloy@gmail.com, mzabaloy@plapiqui.edu.ar (M.S. Zabaloy).

http://dx.doi.org/10.1016/j.fluid.2015.01.020
0378-3812/

maps. They [3] showed that the CMRs have a significant flexibility, which is needed to describe the phase behavior of highly non ideal systems. Later, Cismondi et al. [5] provided an extensive listing on works in the literature which reported experimental data for $CO_2$ + *n*-alkane phase equilibria (carbon number range from 1 to 36). They [5] also proposed the method of predictive correlation, again using the RK-PR EoS combined with temperature dependent CMRs. In the quoted works [3,5] the performance of the CMRs for ternary systems was not explored.

The key features of the (experimental or calculated) phase behavior of a ternary system can be seen at a glance, by the trained eye, over wide ranges of conditions, by looking at the ternary phase equilibrium characteristic map (T-CM) of the system [6,7]. A T-CM is a tool that by reducing the amount of information helps us to increase our understanding of the system behavior.

The fluid phase behavior of ternary systems is related to certain extent to the type of fluid phase behavior of the binary subsystems [6–9]. Pisoni et al. [6,7] have listed types of univariant lines and invariant points that constitute a T-CM, and have calculated them for a number of systems. Their aim [6,7] was to identify patterns of the ternary phase behavior. A point belonging to a phase equilibrium univariant line is an object that has a single degree of freedom. An invariant point has no degrees of freedom. Table 5 provides the names and acronyms of some ternary phase equilibrium univariant lines, and the names, acronyms and physical description of the points they are made of. Table 6 is analogous to Table 5, but it deals with ternary fluid phase equilibrium invariant points. More details on the phenomenology of the phase behavior of ternary systems is provided by Pisoni et al. [7] and by Adrian et al. [1]. It is advised to consider, in particular, Appendix C of Ref. [7], which deals with the fluid phase behavior of ternary systems as seen on sets of Gibbs triangles.

The use of the term T-CM is preferred here over the term "pressure–temperature phase diagram" or "pressure–temperature projection of the phase diagram". The reason is that the words "pressure–temperature" (PT) only mean that certain phase equilibrium line (or hyper-line) is seen in its pressure–temperature projection. For instance, and more specifically, a binary critical line and a binary isopleth phase envelope could both be studied when looking at their PT projections. However, while a binary critical point is univariant, a point of a binary isopleth phase envelope is di-variant. In other words, a binary critical point is a phase equilibrium object that has a single degree of freedom, while a point of a binary isopleth phase envelope has two degrees of freedom. In conclusion, "PT projection" is an ambiguous label, while the words T-CM are not, since we define a T-CM as the set of all phase equilibrium univariant lines and invariant points of a ternary system. A T-CM can be studied by looking at any of its possible projections, e.g, PT, pressure–composition, temperature–composition, pressure–density, etc.

Let us come back, after having mentioned the T-CMs, to the work of Adrian et al. [1], where the performances of a number of mixing rules were compared for highly non ideal ternary systems. They [1] considered $CO_2$ + $H_2O$ + polar solvent systems and focused on the capability of the mixing rules for reproducing T-4PPs, T-CEPs, invariant points (mainly T-TCPs), and ternary two-phase and three-phase equilibria. The authors [1] showed that it is not possible to accurately reproduce ternary phase equilibrium data with cubic equations of state and simple mixing rules when using interaction parameters fit from binary experimental data. See e.g., their Figs. 21 and 23 [1]. In other words, Adrian et al. [1] have shown that, for the highly non-ideal systems studied, the assumption of multicomponent system describability from binary parameters [2] did not perform well.

For a given ternary system, CMRs provide two three-index ternary interaction parameters: one of them influences the mixture attractive energy parameter while the other affects the mixture covolume parameter [2]. By optimizing such ternary parameters, it could be possible to improve the reproduction of ternary experimental data while leaving invariant, i.e, without affecting, the description of the three constituent binary subsystems. In the first part of this work, we examine this approach by studying the system $CO_2$ (1) + *n*-hexadecane (2) + 1,8-octanediol (3), for which we have available both, binary and ternary experimental phase equilibrium data at 393.2 K [10]. For such system, we evaluate the influence of the ternary parameters on the size of ternary two-phase and three-phase equilibrium regions. This study is carried out for varying pressures at constant temperature. It makes possible to establish how helpful changes in ternary parameters are in improving the reproduction of ternary experimental data of a real highly non ideal system. We also study the performance of predicted ternary parameters, which we would need if ternary data were not available.

Before moving forward, let us consider a number of terms related to ternary phase equilibrium objects that partially make the T-CM up [6,7]:

(a) In a ternary critical endpoint (T-CEP), a ternary critical phase is at equilibrium with a ternary non-critical phase. A T-CEP is one of the possible termination points of a continuous set of ternary three-phase equilibria (see Appendix D of Ref. [6] for a discussion on the "termination" nature of a T-CEP).
(b) A ternary critical end line (T-CEL) is a locus of T-CEPs.
(c) At a ternary four-phase (equilibrium) point (T-4PP), four ternary non-critical phases are at equilibrium.
(d) A ternary four-phase (equilibrium) line (T-4PL) is a locus of T-4PPs.
(e) A T-4PL may end at a ternary critical endpoint of a four-phase (equilibrium) line (T-CEP-4PL) where a ternary critical phase is at equilibrium with two ternary non-critical phases.
(f) If, in a continuous set of ternary three-phase equilibria, three phases become critical simultaneously, then, a ternary tricritical endpoint (T-TCEP) (also named ternary tricritical point (T-TCP)) has been reached.

The previous definitions are summarized in Tables 5 and 6.

Notice that using the acronyms T-CEP and T-CEL is, in a way, analogous to use, for binary systems, the pairs of words "critical point" and "critical line". A binary critical point is a constitutive unit of a binary critical line. Similarly, a T-CEP is a constitutive unit of a T-CEL.

As it is well known, a binary critical endpoint (B-CEP) sets, simultaneously, the end of a binary critical line (B-CL) and the end of a binary three-phase equilibrium line (B-3PL). Analogously, a T-CEL sets, simultaneously, the end of a ternary three-phase equilibrium surface and the end of a ternary critical surface [6,7], i.e., a T-CEL is a boundary between both surfaces. This is the reason for replacing the character "P" (point) present within the CEP acronym by the character "L" (line), which leads to the CEL acronym, when going from binary to ternary systems (CEP → CEL).

With the goal of evaluating the effect of ternary interaction parameters over wider ranges of conditions, we perform, in the second part of this work, a parametric study to evaluate the influence of such ternary parameters on calculated (see Tables 5 and 6) T-CELs, T-CEP-4PLs and T-TCPs, i.e, on part of the T-CM, for the system $CO_2$ (1) + $H_2O$ (2) + 2-propanol (3). We do that at set values for the interaction parameters of the corresponding binary subsystems, i.e., $CO_2$ (1) + $H_2O$ (2), $CO_2$ (1) + 2-propanol (3), and $H_2O$ (2) + 2-propanol (3). It is also studied how the changes in the T-CM (caused by the changes in ternary parameters) influence the calculated three-phase equilibria of the mentioned ternary system.

We summarize the goals of this work, as follows:

(a) To study the effect of ternary parameters on the high-pressure isothermal phase behavior of the system $CO_2$ (1) + *n*-hexadecane (2) + 1,8-octanediol (3), comparing calculated and experimental phase equilibria.
(b) To study, over wider ranges of conditions than in item (a), the effect of ternary parameters on calculated T-CELs, T-CEP-4PLs, T-TCPs and ternary three-phase equilibria, for the system $CO_2$ (1) + $H_2O$ (2) + 2-propanol (3).

Both considered ternary systems are highly non-ideal.

## 2. Cubic mixing rules (CMRs)

More specifically cubic mixing and combining rules (CMRs) [2,3,5] are the following:

$$a = \sum_{i=1}^{N}\sum_{j=1}^{N}\sum_{k=1}^{N} x_i x_j x_k a_{ijk} \quad (1)$$

$$a_{ijk} = a^0_{ijk}(1 - k_{ijk}) \quad (2)$$

$$a^0_{ijk} = (a_i a_j a_k)^{(1/3)} \quad (3)$$

$$b = \sum_{i=1}^{N}\sum_{j=1}^{N}\sum_{k=1}^{N} x_i x_j x_k b_{ijk} \quad (4)$$

$$b_{ijk} = b^0_{ijk}(1 - l_{ijk}) \quad (5)$$

$$b^0_{ijk} = \frac{b_i + b_j + b_k}{3} \quad (6)$$

where $N$ is the number of components in a multicomponent mixture, $a_i$, $b_i$ and $x_i$ are, for component $i$, the EOS attractive energy parameter, the EOS repulsive co-volume parameter and the mole fraction in the multicomponent system, respectively, $k_{ijk}$ and $l_{ijk}$ are respectively the energy interaction parameter and the covolume interaction parameter. For a binary system of components 1 and 2, the cubic mixing rules provide four independent three-index binary interaction parameters, i.e., $k_{112}$, $k_{122}$, $l_{112}$ and $l_{122}$. Thus, the number of available binary (three index) interaction parameters in cubic mixing rules doubles the number of binary (two-index) interaction parameters that quadratic mixing rules provide. The conventional quadratic mixing rules are a particular case of cubic mixing rules [2]. For ternary or higher systems, Eqs. (2) and (5) require three-index ternary parameters (e.g, $k_{123}$ and $l_{123}$ for the case of a ternary system). Such ternary parameters can be either regressed from experimental information on ternary systems or predicted from three-index binary parameters obtained from experimental data on binary systems [2]. The potential correlation of ternary data by fitting ternary interaction parameters, while leaving invariant the description of the constituent binary systems, makes the CMRs appealing. In Appendix A, a brief discussion is provided on the composition dependence of virial coefficients obtained from a chosen combination of equation of state and mixing rules.

The system $CO_2$ (1) + *n*-hexadecane (2) + 1,8-octanediol (3) was experimentally studied by Spee and Schneider [10], who reported phase equilibrium data at 393.2 K for the ternary system and for the three binary subsystems, in the pressure range from 10 MPa (100 bar) to 100 MPa (1000 bar). At 393.2 K, the binary system $CO_2$ (1) + *n*-hexadecane (2) has a critical point at about 256 bar [10]. At 393.2 K the system $CO_2$ (1) + 1,8-octanediol (3) presents liquid–liquid equilibrium in the pressure range considered in this work (pressure greater than or equal to 225 bar). This conclusion comes from our correlation of the $CO_2$ (1) + 1,8-octanediol (3) fluid–fluid equilibrium data at 393.2 K, after looking at the (not shown in this work) values of the calculated mass densities of the phases at equilibrium. At 393.2 K, the system *n*-hexadecane (2) + 1,8-octanediol (3) also presents liquid–liquid equilibrium in the pressure range studied in Ref. [10]. Using the PR-EOS [11], coupled to CMRs, we obtained in this work a (not shown) very good correlation of the experimental data of the three binary subsystems. Table 1 reports the binary parameter values, and Table 2 reports the pure compound parameters that we used for the PR-EOS [11].

**Table 1**
Binary three-index and nominal ternary three-index interaction parameters at 393.2 K used in this work for the PR-EOS [11] coupled to CMRs [2,3,5] for the system $CO_2$ (1) + *n*-hexadecane (2) + 1,8-octanediol (3).

| Parameter | Value | Parameter | Value |
|---|---|---|---|
| Three-index binary parameters[a] | | | |
| $k_{112}$ | −0.26264 | $l_{112}$ | 0.16014 |
| $k_{122}$ | −0.44454 | $l_{122}$ | 0.14698 |
| $k_{113}$ | −0.09550 | $l_{113}$ | 0.10495 |
| $k_{133}$ | −0.23524 | $l_{133}$ | 0.11093 |
| $k_{223}$ | 0.11000 | $l_{223}$ | 0.01042 |
| $k_{233}$ | 0.02074 | $l_{233}$ | 0.00030 |
| Nominal three-index ternary parameters | | | |
| $k_{123}$ | −0.3625460[b] | $l_{123}$ | 0.1201179[c] |

[a] Fitted in this work from binary phase equilibrium data from Ref. [10].
[b] Predicted from Eq. (30) of Zabaloy [2].
[c] Predicted from Eq. (30) of Zabaloy [2] but using such equation with $b_{ijk}$ of Eq. (5) in place of $a_{ijk}$ of Eq. (2).

At 393.2 K, the ternary system $CO_2$ (1) + *n*-hexadecane (2) + 1,8-octanediol (3) presents, at a given pressure in the range from 256 bar to 500 bar, a single two-phase region (e.g., Fig. 1) connecting the two immiscible binary subsystems, i.e., the systems $CO_2$ (1) + 1,8-octanediol (3) and *n*-hexadecane (2) + 1,8-octanediol (3); while, in the range from 100 bar to 256 bar, where the system $CO_2$ (1) + *n*-hexadecane (2) gives vapor–liquid splits, the ternary system presents, at a given pressure, three two-phase regions and a single three-phase region (e.g., Fig. 4) [10]. Besides binary three-index parameters, Table 1 reports ternary three-index parameters predicted [2], for this system, based on the assumption of mixture molar volume invariance [2]. This assumption [12] leads to a classification that distinguishes between variant and invariant properties of mixtures. Ref. [12] has generalized the considerations by Michelsen and Kistenmacher [13]. These authors defined [13]

**Table 2**
Pure compound parameters used in this work for the PR-EOS [11] and/or for the SRK-EOS [16].

| Compound | Critical temperature (K) | Critical pressure (bar) | Acentric factor |
|---|---|---|---|
| Carbon dioxide[a] | 304.21 | 73.83 | 0.22362 |
| 2-Propanol[a] | 508.30 | 47.64 | 0.66690 |
| Water[a] | 647.13 | 220.55 | 0.34490 |
| *n*-Hexadecane[a] | 723.00 | 14.00 | 0.71740 |
| 1,8-Octanediol[b] | 709.46 | 26.71087 | 1.13320651 |

[a] From DIPPR [21] data base.
[b] Obtained in this work by interpolating DIPPR [21] information on components 1,4-butanediol; 1,5-pentanediol; 1,6-hexanediol and decan-1,10-diol.

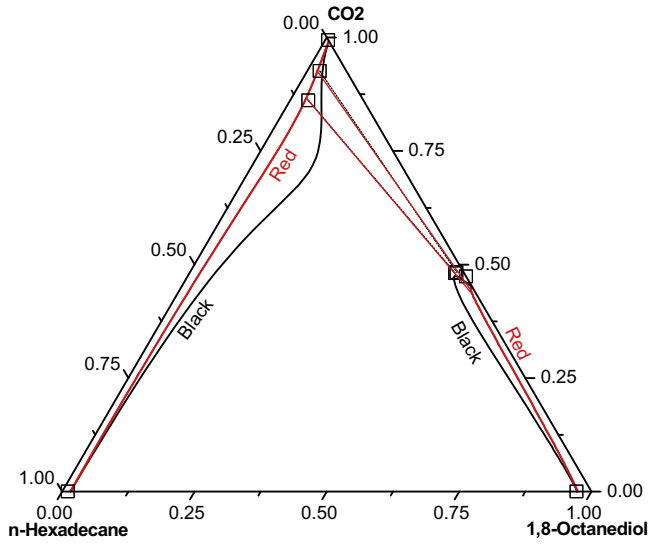


**Fig. 1.** Fluid–fluid equilibrium for the system $CO_2$ (1) + *n*-hexadecane (2) + 1,8-octanediol (3) at 400 bar and 393.2 K (concentration scale: mole fraction). Squares: experimental binary or ternary two-phase compositions [10]. Straight black dashed lines: experimental ternary two-phase tie-lines [10]. Black solid curves: PR-EOS + CMRs with Tables 1 and 2 parameters. Red solid curves: PR-EOS + CMRs with Tables 1 and 2 parameters except for $k_{123}$ ($k_{123} = -0.26254$). Red solid straight lines: calculated ternary two-phase tie-lines ($k_{123} = -0.26254$). (For interpretation of the references to color in this figure legend, the reader is referred to the web version of this article.)

the afterwards called [14] "Michelsen–Kistenmacher syndrome". The predicted ternary three-index interaction parameters reported in Table 1 come from a formula [2] that is free from such syndrome.

Such predicted values, which we name "nominal" values, would be used for ternary and higher systems if the ternary experimental data were not available. Our goal for this ternary system is to evaluate how the model departs from the experimental data as the three-index ternary parameters change.

Di Andreth [15] studied the phase behavior of the ternary system $CO_2$ (1) + $H_2O$ (2) + 2-propanol (3) over wide ranges of temperature and pressure. He fit phase equilibrium experimental data for such system using the model SRK-EOS + QMRs [16]. Table 2 reports the pure compound parameters used in this work, which correspond to the system $CO_2$ (1) + $H_2O$ (2) + 2-propanol (3). For the binary subsystems $CO_2$ (1) + $H_2O$ (2), $CO_2$ (1) + 2-propanol (3) and $H_2O$ (2) + 2-propanol (3), we obtained, using the SRK-EOS + CMRs, values for the binary three-index interaction parameters. They are reported in Table 3. These parameters qualitatively reproduce the topology of the binary univariant lines (in their pressure–temperature projections) that can be computed using also the SRK-EOS, but coupled to QMRs, with the (two-index) binary interaction parameters reported by Di Andreth [15]. Examples of binary univariant lines are critical lines, liquid–liquid–vapor lines and azeotropic lines; and examples of a binary invariant points are binary critical end points and critical azeotropic points [8,9].

**Table 3**
Binary three-index interaction parameters used in this work for the SRK-EOS [16] coupled to CMRs [2,3,5] for the $CO_2$ (1) + $H_2O$ (2) + 2-propanol (3) system.

| | | | |
|---|---|---|---|
| $k_{112}$ | 0.10700 | $l_{112}$ | −0.020 |
| $k_{122}$ | −0.06700 | $l_{122}$ | 0.009 |
| $k_{113}$ | −0.02499 | $l_{113}$ | 0.001 |
| $k_{133}$ | −0.05400 | $l_{133}$ | 0.012 |
| $k_{223}$ | −0.13000 | $l_{223}$ | 0.060 |
| $k_{233}$ | −0.11000 | $l_{233}$ | 0.004 |

**Table 4**
Combinations of values of the ternary three-index interaction parameters ($k_{123}$ and $l_{123}$) considered in this work for computing some T-CELs and some three-phase equilibria for the $CO_2$ (1) + $H_2O$ (2) + 2-propanol (3) system using the SRK-EOS [16] coupled to CMRs [2,3,5].

| Cases | $k_{123}$ | $l_{123}$ |
|---|---|---|
| Case 1 | 0.00 | 0.00 |
| Case 2 | 0.13 | −0.14 |
| Case 3 | −0.25 | 0.20 |

Appendix C presents the calculated phase behavior characteristic maps, in their pressure–temperature projections, for the binary systems $CO_2$ (1) + $H_2O$ (2), $CO_2$ (1) + 2-propanol (3) and $H_2O$ (2) + 2-propanol (3).

Our goal in this case is to carry out a parametric study to evaluate the effect of the three-index ternary interaction parameters, of the CMRs, on the ternary fluid phase equilibria, over wide ranges of conditions, for system $CO_2$ (1) + $H_2O$ (2) + 2-propanol (3). The changes in the three-index ternary interaction parameters will be done keeping the two-index binary interaction parameters fixed at the values given in Table 3. In this second part of the present work, it is not our goal to reproduce experimental information on ternary phase equilibria, but to explore to which extent we could manipulate the computed ternary phase equilibrium by varying the values of the three-index ternary parameters. Table 4 reports the ternary three-index interaction parameters $k_{123}$ and $l_{123}$ used in this work to compute, for three different cases, ternary univariant lines and ternary three-phase equilibria for the $CO_2$ (1) + $H_2O$ (2) + 2-propanol (3) system.

## 3. Results and discussion

### *3.1. Effect of three-index ternary interaction parameters on the description of the phase equilibria of system $CO_2$ (1) + n-hexadecane (2) + 1,8-octanediol (3)*

In this work, we performed fluid phase equilibria calculations by solving the isofugacity condition, for the ternary system $CO_2$ (1) + *n*-hexadecane (2) + 1,8-octanediol (3), and also for the corresponding binary subsystems, at 393.2 K, using the PR-EOS [11] coupled to CMRs [2,3,5] with the binary interaction parameter values of Table 1 and the pure compound parameters of Table 2. We compared the model results with the experimental data of Spee and Schneider [10].

Fig. 1 shows the fluid–fluid equilibrium for the system $CO_2$ (1) + *n*-hexadecane (2) + 1,8-octanediol (3) at 400 bar and 393.2 K. The concentration scale of Fig. 1 is the "mole fraction" scale. The squares and the black dashed (straight) tie lines correspond to the experimental data of Spee and Schneider [10]. Three squares are very close to each other. Two of them are located also very close to the $CO_2$ (1) + 1,8-octanediol (3) side of the Gibbs triangle and the third one on such side. This last point is part of a binary datum, and the other two are ternary data. The black solid curves correspond to the PR-EOS [11] (with Table 2 pure compound parameters) coupled to CMRs with Table 1 parameters. Thus, for the black lines, the ternary parameters have the predicted (not fitted) values of Table 1. The black lines connect the miscibility limits of the *n*-hexadecane (2) + 1,8-octanediol (3) binary to those of the $CO_2$ (1) + 1,8-octanediol (3) system (the binary $CO_2$ (1) + *n*-hexadecane (2) is homogeneous at 400 bar and 393.2 K, Fig. 1). It is therefore clear that the black lines are the boundaries of a two-phase equilibrium region which is continuous from the *n*-hexadecane (2) + 1,8-octanediol (3) binary to the $CO_2$ (1) + 1,8-octanediol (3) binary. The black curves give the same qualitative behavior than that of Fig. 5 of the paper by Spee and Schneider ([10] p. 270). From

Fig. 1, it is clear that if we use predicted (i.e., "nominal") ternary parameters we obtain, for the phase with the lowest 1,8-octanediol (3) concentration, a curve (left black curve) closer to the 1,8-octanediol (3) vertex than the experimental curve. Notice that no tie-lines are shown for the case of the nominal ternary parameters.

Fig. 1 also presents calculation results (red curves and red tie-lines) that we carried out using the nominal value of parameter $l_{123}$ (Table 1) and setting $k_{123} = (-0.26254)$. Such value for $k_{123}$ came from forcing a good agreement between the ternary experimental data at lower 1,8-octanediol (3) concentration and the model. Such forced agreement is evident in Fig. 1 from comparing the red curve located close to the $CO_2$ (1) + *n*-hexadecane (2) side of the Gibbs triangle with the experimental ternary data (squares).

Notice in Fig. 1 that the miscibility limits for the binary subsystems are the same both, for the nominal value of $k_{123}$ (−0.362546, Table 1) and for the fitted value (−0.26254). Since $k_{123} = (-0.26254) > k_{123}^{\text{nominal}} = -0.362546$, the nominal case corresponds to greater values for the attractive mixture parameter (Eqs. (1)–(3)). From this, we expect a higher miscibility for the ternary system modeled using the nominal value for $k_{123}$. Fig. 1 confirms such expectation: we observe that the red curves are located closer to the non horizontal sides of the Gibbs triangle than the black curves do.

Fig. 2 is analogous to Fig. 1. The black curves in Fig. 2 are identical to the black curves in Fig. 1, i.e., they correspond to the nominal case (Table 1). We obtained the red curves and (straight) tie-lines in Fig. 2 differently from the case of Fig. 1, i.e., by fitting the $l_{123}$ parameter while keeping parameter $k_{123}$ set at its nominal value. The red curves in Fig. 2 have a qualitative behavior quite similar to that of the red lines in Fig. 1. We see however that the immiscibility region corresponding to the red curves of Fig. 2 is slightly wider than the immiscibility region of the red curves of Fig. 1. This is noticeable by looking, e.g., at the left red curves in Figs. 1 and 2.

The fitted value of $l_{123}$ (0.00979) is less than its nominal value (0.1201179, Table 1), which implies higher values for the mixture repulsive parameter (Eqs. (4)–(6)). This is associated to an expectation of a wider immiscibility region for the fitted parameter, which we verify in Fig. 2. In conclusion, we can produce similar effects by decreasing the ternary attractive mixture parameter "*a*" (Fig. 1) or by increasing the ternary repulsive mixture parameter "*b*" (Fig. 2). This is consistent with results previously found in a proto-modeling study [17] related to the seminal work by Scott and van Konynenburg [9]. We stress that the (straight) tie-lines in Figs. 1 and 2 correspond to two-phase equilibria (not to three-phase equilibria).

Fig. 3 presents our calculation results for the fluid–fluid equilibrium of system $CO_2$ (1) + *n*-hexadecane (2) + 1,8-octanediol (3) at 500 bar and 393.2 K, at varying $k_{123}$ values, again for the PR-EOS [11] with CMRs [2]. In Fig. 3, rather than reproducing experimental data, what we do is to illustrate the high level of flexibility associated to the ternary parameters of the cubic mixing rules. We see that by decreasing parameter $k_{123}$, i.e., by increasing the mixture parameter "*a*" (Eq. (2)), we are able to produce an evolution from a continuous two-phase region connecting the two binary immiscible subsystems (blue lines), to a situation where we have two disconnected two-phase regions (black lines). In this last case, a given two-phase region stems from a binary fluid–fluid equilibrium point and ends at a critical point (not identified in Fig. 3). The transition between the two extreme cases of Fig. 3 requires that at intermediate $k_{123}$ values the ternary miscibility boundary lines of the continuous two-phase region (blue lines) get increasingly closer, as illustrated by the red lines in Fig. 3. Besides, Fig. 3 shows, perhaps more clearly than the previous figures, that the changes inside the Gibbs triangle happen, for CMRs, without changes in the binary phase equilibria represented on the sides of the triangle, i.e., the description of the binary subsystems remains invariant with respect to changes in the ternary three-index parameters if we keep constant the binary three-index parameters (and also the pure compound parameters).

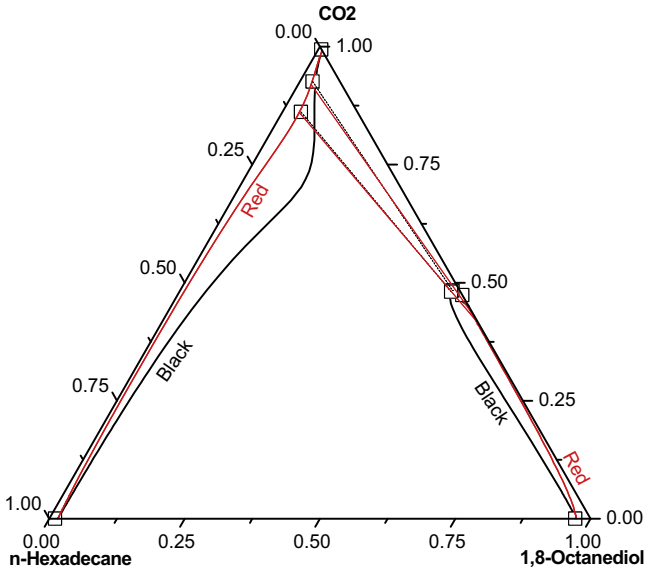


**Fig. 2.** Fluid–fluid equilibrium for the system $CO_2$ (1) + *n*-hexadecane (2) + 1,8-octanediol (3) at 400 bar and 393.2 K (concentration scale: mole fraction). Squares: experimental binary or ternary two-phase compositions [10]. Straight black dashed lines: experimental ternary two-phase tie-lines [10]. Black solid curves: PR-EOS + CMRs with Tables 1 and 2 parameters. Red solid curves: PR-EOS + CMRs with Tables 1 and 2 parameters except for $l_{123}$ ($l_{123} = 0.00979$). Red solid straight lines: calculated ternary two-phase tie-lines ($l_{123} = 0.00979$). (For interpretation of the references to color in this figure legend, the reader is referred to the web version of this article.)

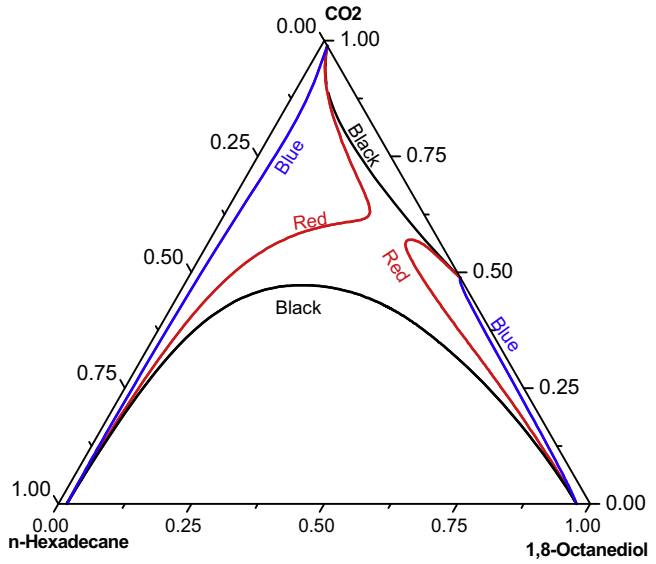


**Fig. 3.** Effect of the $k_{123}$ parameter on the calculated ternary fluid–fluid equilibrium for the system $CO_2$ (1) + *n*-hexadecane (2) + 1,8-octanediol (3) at 500 bar and 393.2 K (concentration scale: mole fraction). Model: PR-EOS + CMRs and Tables 1 and 2 parameters except for blue solid curves, $k_{123} = -0.26254$; red solid curves, $k_{123} = -0.40254$; black solid curves, $k_{123} = -0.46254$. (For interpretation of the references to color in this figure legend, the reader is referred to the web version of this article.)

Fig. 4 presents the fluid–fluid equilibrium for the system $CO_2$ (1) + *n*-hexadecane (2) + 1,8-octanediol (3) at 225 bar and 393.2 K. The system pressure, i.e., 225 bar, is below 256 bar, i.e., below the critical pressure of the binary system $CO_2$ (1) + *n*-hexadecane (2) at 393.2 K. Therefore, the three binary subsystems present two-phase equilibrium under the conditions of Fig. 4, at which, Spee and Schneider [10] experimentally detected a three phase ternary region (squares not located on the sides of the Gibbs triangle and straight dashed tie-lines in Fig. 4). Notice that in Fig. 4, we actually see two replicates of a single three-phase equilibrium experiment. Fig. 4 shows that the PR-EOS [11] + CMRs [2] with nominal ternary three-index interaction parameter values, predicts three two-phase regions: each of them ends at one of the sides (tie-lines) of the calculated three-phase triangle. Such three-phase region is narrower than the experimental one. Fig. 5 (225 bar) shows that the agreement between the model and the experiments, at three-phase equilibrium, significantly improves if we use for $k_{123}$ the value that we previously fit from ternary two-phase data at 400 bar (Fig. 1). See Appendix B for a better visualization of the information already given in Fig. 5.

The results shown in this section provide evidence of the improvement that can be gained in the quantitative description of ternary phase equilibria by resorting to three-index ternary parameters set at convenient values.

### 3.2. Effect of three-index ternary interaction parameters over wide ranges of conditions: system $CO_2$ (1) + $H_2O$ (2) + 2-propanol (3)

In Section 3.1, we have considered isothermal (single temperature value) equilibria and a range of pressures. In contrast, the present section deals with wide ranges of temperature (and also of pressure). The effect of a given parameter on the calculated phase behavior given by an EOS model can be seen at a glance by looking at corresponding series of phase behavior T-CMs, or at least at series of some of the elements of such T-CMs. The present section reports a parametric study whose goal is to scrutinize the influence of three-index ternary parameters on the shape and extent of calculated T-CELs and related three-phase equilibria. Since T-CELs are boundaries of ternary three-phase surfaces, their extent are in part indicative of the extent of such regions.

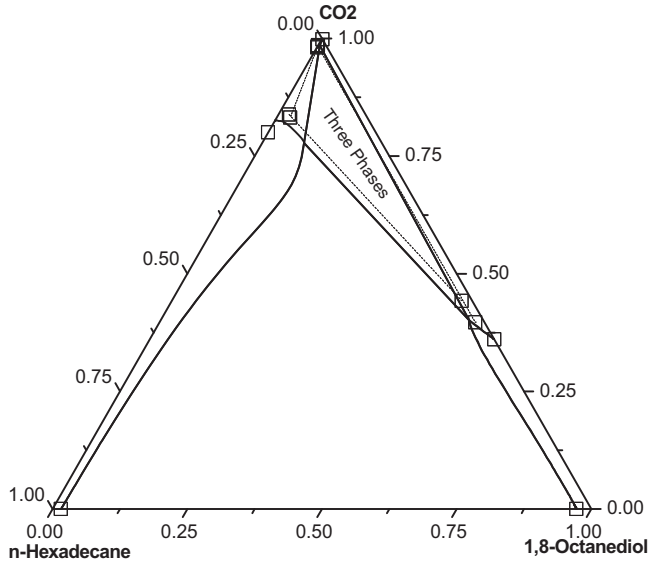


**Fig. 4.** Fluid–fluid equilibrium for the system $CO_2$ (1) + *n*-hexadecane (2) + 1,8-octanediol (3) at 225 bar and 393.2 K (concentration scale: mole fraction). Squares on the sides of the Gibbs triangle: experimental binary two-phase compositions [10]. Squares inside the Gibbs triangle: experimental ternary three-phase compositions (two replicates) [10]. Straight dashed lines: experimental ternary three-phase tie-lines [10]. Solid lines and curves: PR-EOS + CMRs with Tables 1 and 2 parameters. These lines and curves indicate three ternary two-phase regions and a single ternary three-phase region.

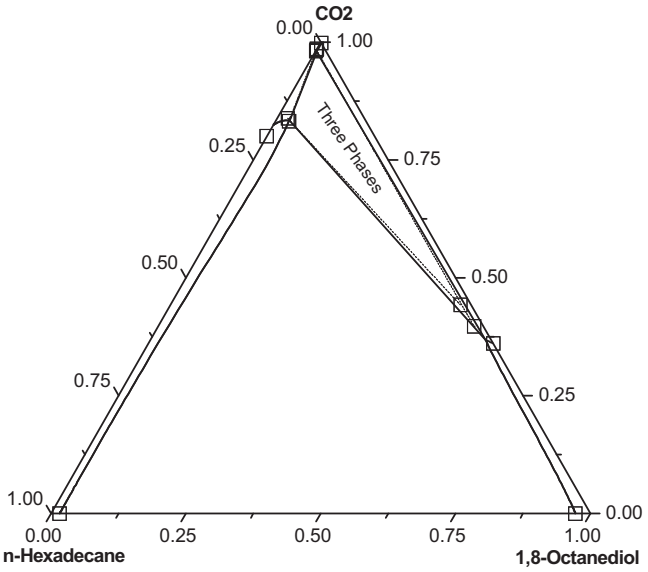


**Fig. 5.** Caption as in Fig. 4, except that $k_{123}$ has in this case been set equal to that of Fig. 1, i.e., $k_{123} = -0.26254$.

T-CELs for system $CO_2$ (1) + $H_2O$ (2) + 2-propanol were computed using the SRK-EOS [16] + CMRs [2], for the three cases defined in Table 4, while keeping fixed the binary parameters of Table 3. The calculation procedures have been described elsewhere [6,7].

Fig. 6 presents the pressure–temperature projection of a part of the T-CMs for the three cases of Table 4. The system is $CO_2$ + $H_2O$ + 2-propanol. This figure shows that the topology of the computed T-CELs strongly depends on the values of parameters $k_{123}$ and $l_{123}$ (the binary phase behavior is the same for all three cases). It is again suggested the reading of Appendix C of Ref. [7] for a better understanding on what T-CELs mean.

Fig. 7a shows "case 1" of Table 4 ($k_{123}$ and $l_{123}$ are both equal to zero). The computed T-CEL originates at a binary critical endpoint (B-CEP, empty circle) of the subsystem $CO_2$ (1) + $H_2O$ (2) and ends at a T-TCP. Ref. [6] describes how the imminency of a T-TCP is detected while computing a T-CEL, and it also gives an account of

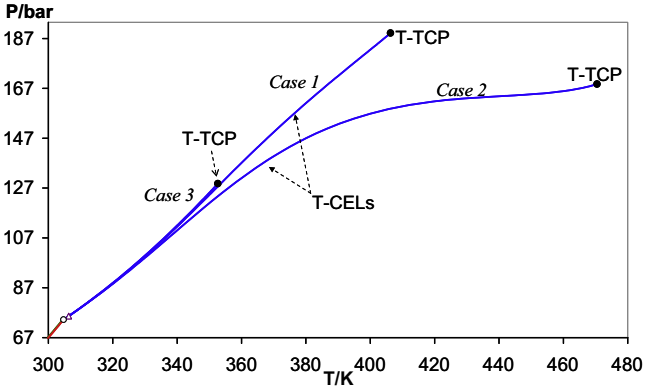


**Fig. 6.** Pressure–temperature projection of a part of the ternary characteristic map (T-CM) calculated for the $CO_2$ + $H_2O$ + 2-propanol system using the SRK-EOS coupled to CMRs (parameters reported in Tables 2–4). Cases 1–3 (Table 4). Acronyms: T-CEL: ternary critical end line; T-TCP: ternary tricritical point.

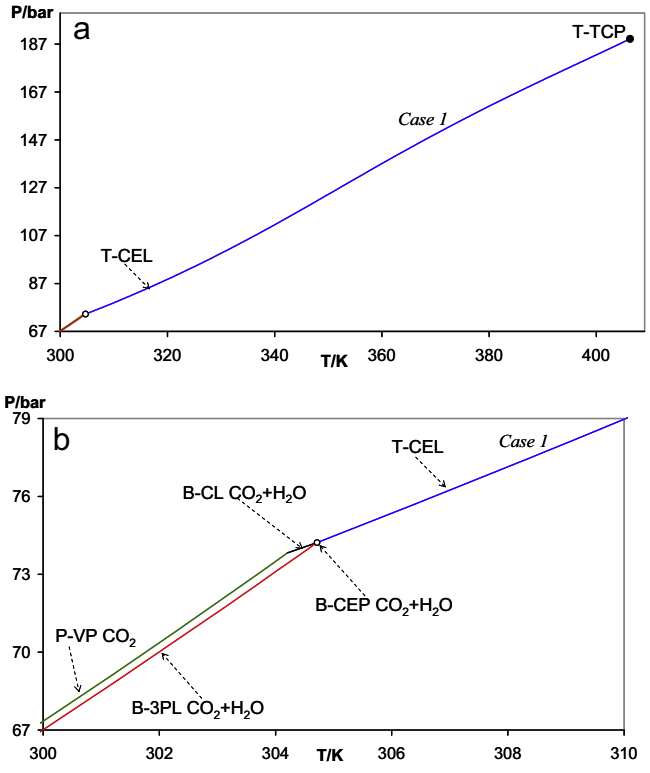


**Fig. 7.** (a) Caption as in Fig. 6, except that only case 1 (Table 4) is shown. (b) Zoom of (a) (case 1, Table 4). Acronyms: P-VP: pure compound vapour pressure; B-3PL: binary three phase line; B-CL: binary critical line; B-CEP: binary critical end point; T-CEL: ternary critical end line.

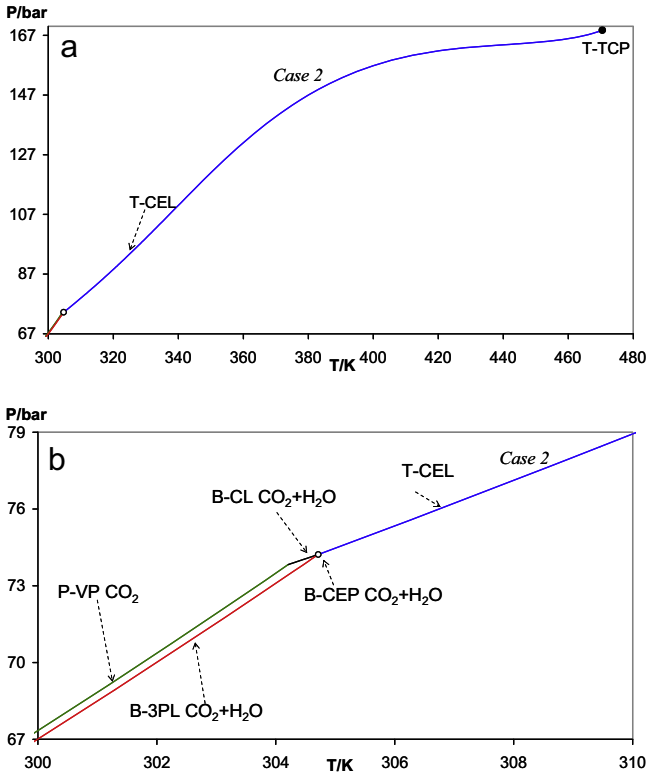


**Fig. 8.** (a) Caption as in Fig. 6, except that only case 2 (Table 4) is shown. (b) Zoom of (a) (case 2, Table 4). Acronyms as in Fig. 7. Acronyms: T-CEL: ternary critical end line; T-TCP: ternary tricritical point.

the process of rigorously solving the system of equations corresponding to the tricritical conditions. A brief discussion on the nature of tricritical points is provided in Appendix D.

Fig. 7b is a zoom of Fig. 7a. It shows the pure $CO_2$ vapor pressure line (pure liquid–vapor equilibrium). It also shows, for the binary subsystem $CO_2$ (1) + $H_2O$ (2), a critical line (B-CL), the three-phase equilibrium line (B-3PL), and the B-CEP (empty circle). All binary and unary objects were computed according to Ref. [18]. In Fig. 7b, it is more clearly seen how the computed T-CEL originates at the B-CEP.

Fig. 8a shows "case 2" of Table 4 for which $k_{123}$ is positive and $l_{123}$ is negative. Fig. 8b is a zoom of Fig. 8a covering the narrower temperature range from 300 to 310 K. The T-CEL originates at the B-CEP of system $CO_2$ (1) + $H_2O$ (2) (empty circle) and ends at a T-TCP. The temperature range of existence of the "case 2/T-CEL" (Fig. 8a) is significantly wider than that of the "case 1/T-CEL" (Fig. 7a). On the other hand, the "case 1/T-CEL" covers a pressure range wider than that of "case 2/T-CEL" by approximately 20 bar (Fig. 6). Finally, the pressure–temperature projection of the "case 2/T-CEL" has a higher level of non linearity than that of the "case 1/T-CEL" (Fig. 6).

Fig. 9a presents "case 3" of Table 4 for which $k_{123}$ is negative and $l_{123}$ is positive. We see two T-CELs. One of them has a narrow temperature range. It originates at the B-CEP (empty circle) and ends at a T-CEP-4PL (triangle in Figs. 6 and 9a and b). The second T-CEL emerges at the T-CEP-4PL and extends up to a T-TCP. The presence of a T-CEP-4PL implies a more complex qualitative behavior than those of cases 1 and 2. Such T-CEP-4PL indicates the existence of a T-4PL (see Tables 5 and 6) [6,7], which is not shown in this work. The T-4PL originates at the T-CEP-4PL [6,7]. Besides, the temperature range of the "case 3" T-CELs is much narrower than those of "case 1/T-CEL" and "case 2/T-CEL", as clearly shown in Fig. 6.

Fig. 10a exhibits the same T-CELs of Fig. 6 but in their temperature–molar volume projections. In general, we see in Fig. 10a, for a given T-CEL and given temperature, the molar volumes of two phases at equilibrium (the two phases of the chosen T-CEP, Table 5). The exception is the T-CEP-4PL (triangles) where three phases are at equilibrium (see Table 6). Three out of the four T-CELs originate at the B-CEP of system $CO_2$ (1) + $H_2O$ (2), which in this projection is indicated as two empty circles (Fig. 10a and b). Fig. 10a shows important differences among the topologies of the T-CELs. Such differences are promoted by the differences in the values of the three-index ternary parameters $k_{123}$ and $l_{123}$ corresponding to cases 1–3 (Table 4). In the projection of Fig. 10a, the three clearly visible T-CELs present a highly non-linear behavior, mainly for case 2. In Fig. 10a and b, it is again possible to visualize that changes in parameters $k_{123}$ and $l_{123}$ may influence not only the values of the phase equilibrium variables of the ternary system but also the nature of such phase equilibria, giving raise, e.g., to the appearance of a T-4PL in "case 3", while such type of line is not observed in cases 1 and 2. Notice that although four T-CELs are represented in Fig. 10b, it is difficult to visualize one of them due to its relatively narrow temperature range of existence.

Since a T-CEL is a boundary between a ternary three-phase equilibrium surface and a ternary critical surface [6,7], the topology and ranges of existence of a T-CEL partially influences the topology, and the ranges of existence, of both mentioned surfaces. For instance, Fig. 6 tells that one of the boundaries of the three-phase surface of "case 2" covers a wider temperature range than the corresponding boundary of the three-phase surface of "case 1". The first mentioned boundary is the "case 2/T-CEL", and the second one is the "case 1/T-CEL".

To more completely scrutinize how the changes in the values of the ternary three-index parameters promote changes in the

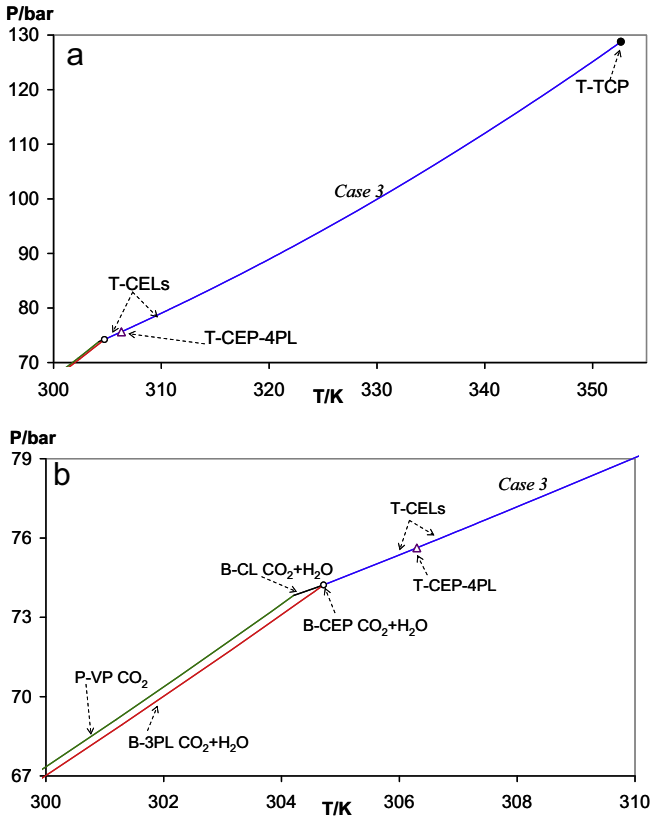


**Fig. 9.** (a) Caption as in Fig. 6, except that only case 3 (Table 4) is shown. (b) Zoom of (a) (case 3, Table 4). Acronyms as in Figs. 7 and 9. Acronyms: T-CELs: ternary critical end lines; T-TCP: ternary tricritical point; T-CEP-4PL: ternary critical end point of a four phase line.

calculated ternary phase equilibria, two isobaric ternary three-phase equilibrium lines (or hyper-lines, T-3PLs) were calculated in this work over relatively wide temperature ranges. They correspond to cases 1 and 2 of Table 4.

Fig. 11 shows the temperature–molar volume projection of a T-3PL, computed at a constant pressure of 73 bar, for "case 1" (Table 4). At a given temperature, it is possible to read from Fig. 11 the molar volume for each of the three equilibrium phases. The three branches of Fig. 11 are all part of the same isobaric three-phase hyper-line. This multiplicity of coordinates (molar volumes, pressure, temperature, and phase compositions, etc.) that describe a ternary three-phase equilibrium point (or hyper-point) is the reason that makes the word "hyper-line" more appropriate than the word "line". The T-3PL originates at low temperature, more specifically at a binary three-phase equilibrium point (B-3PP, empty circles) of the subsystem $CO_2$ (1) + $H_2O$ (2). This B-3PP could be visualized, for instance in Fig. 9b, as the intersection point of a constant pressure line at 73 bar with the line labeled "B-3PL". The T-3PL extends up to a T-CEP that belongs to a T-CEL (not computed in this work) which is not the same than the T-CEL shown for this case (case 1) in Fig. 7a and b (a given ternary system may have several T-CELs, [6,7]). The liquid phases L1 and L2 become critical at about 321 K (left full circle in Fig. 11). Phase L3 is a vapor phase.

Fig. 12 shows in a 3D space the temperature–mole fraction projection of the same calculated ternary three-phase line of Fig. 11. The phase compositions at a given temperature of a three-phase equilibrium hyper-point are obtained by intersecting a constant temperature (horizontal) plane with lines L1, L2 and L3. In this figure, the $CO_2$ (1) + $H_2O$ (2) B-3PP of Fig. 11, where the three-phase hyper-line originates, is also visualized (empty circles). From Fig. 12, it should be clear that two of the phases of the B-3PP are highly concentrated in $CO_2$.

The three-phase equilibrium has a continuous evolution from the B-3PP to a T-CEP where the compositions of phases L1 and L2 become identical due to the criticality condition for one of the phases of the T-CEP. Fig. 12 illustrates the rationale behind part of the name "T-CEP": it is an hyper-point where a ternary three-phase equilibrium locus ends. The label T-3PL applies to the set made of the three red curves in Fig. 12, since such three red lines make a single (constant pressure) three-phase hyper-line [6,7]. Actually, such hyper-line also includes additional information, e.g., the red lines in Fig. 11.

In Fig. 11 and indeed in Fig. 12, it can be seen that the temperature range of existence of the ternary three-phase equilibrium at 73 bar is approximately 18 K wide.

Fig. 13 is analogous to Fig. 11. The difference is that the ternary three-index parameters are those of "case 2" (Table 4) for Fig. 13. The T-3PL in Fig. 13 (case 2) originates at the same binary $CO_2$ (1) + $H_2O$ (2) three-phase equilibrium point than the T-3PL in Fig. 11 (case 1). The T-3PL in Fig. 13 does not have a T-CEP within the temperature range of Fig. 13. Such range is significantly wider than that of Fig. 11 (range width about 44 K in Fig. 13 vs. 18 K in Fig. 11).

Fig. 14 relates to Fig. 13 in a way analogous to the way in which Figs. 11 and 12 relate. The qualitative behavior in Fig. 14 is similar to

**Table 5**
Ternary fluid phase equilibrium univariant lines [1,6,7,15].

| Line acronym | Line name | Point acronym | Point[a] name | Point physical description |
|---|---|---|---|---|
| T-4PL | Ternary four- phase (equilibrium) line | T-4PP | Ternary four-phase (equilibrium) point | Four ternary non-critical phases are at equilibrium. |
| T-AL | Ternary azeotropy line | T-AP | Ternary azeotropic point | A ternary liquid phase and a ternary vapor phase having identical composition are at equilibrium. |
| T-CEL | Ternary critical end line | T-CEP | Ternary critical endpoint | A ternary critical phase is at equilibrium with a ternary non-critical phase. |

[a] The point has a single degree of freedom.

**Table 6**
A couple of ternary fluid phase equilibrium invariant points [1,6,7,15].

| Point acronym | Point[a] name | Point physical description |
|---|---|---|
| T-CEP-4PL | Ternary critical endpoint of a four-phase (equilibrium) line | A ternary critical phase is at equilibrium with two ternary non-critical phases. |
| T-TCEP or T-TCP | Ternary tricritical endpoint or ternary tricritical point | Three ternary phases at equilibrium become critical simultaneously at the T-TCP. |

[a] The point has no degrees of freedom.

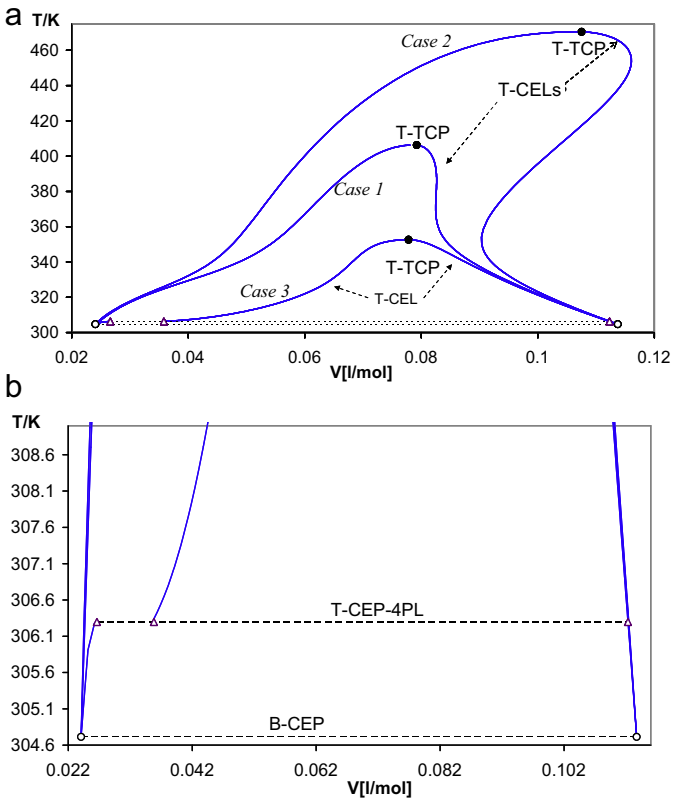


**Fig. 10.** (a) Temperature–molar volume projection of a part of the ternary characteristic map (T-CM) calculated for the $CO_2 + H_2O$ + 2-propanol system using the SRK-EOS coupled to CMRs (parameters reported in Tables 2–4). Cases 1–3 (Table 4). The triangles are the molar volumes of the critical and the two non-critical phases at equilibrium at the T-CEP-4PL. The circles are the molar volumes of the critical and the non critical phases at equilibrium of the ($CO_2 + H_2O$) B-CEP. Acronyms: T-CELs: ternary critical end lines; T-TCP: ternary tricritical point. (b) Zoom of (a) (cases 1–3, Table 4). Acronyms: B-CEP: binary critical end point; T-CEP-4PL: ternary critical end point of a four phase line.

the one in Fig. 12. Figs. 13 and 14 suggest that phases L1 and L2 tend to become identical, i.e., critical, with increasing temperature, and consequently that the ternary three-phase locus would terminate

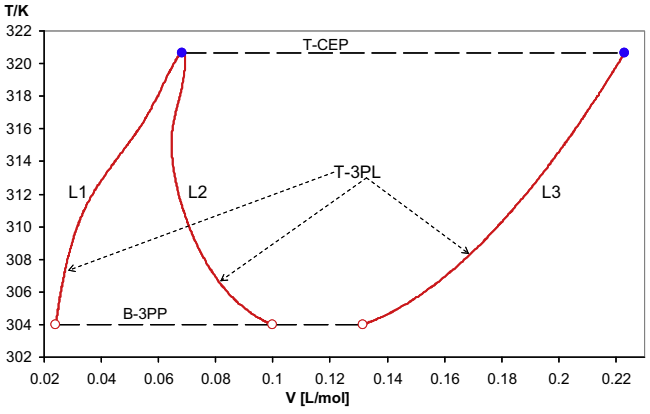


**Fig. 11.** Temperature–molar volume projection of a ternary three-phase equilibrium line calculated for the $CO_2 + H_2O$ + 2-propanol system at $P = 73$ bar, using the SRK-EOS coupled to CMRs (parameters reported in Tables 2–4). Case 1 (Table 4). Acronyms: B-3PP: binary three phase point (empty circles); T-CEP: ternary critical end point (blue full circles); T-3PL: ternary three phase line. The L1, L2 and L3 labels identify each phase in equilibrium. L3 is a vapor phase. (For interpretation of the references to color in this figure legend, the reader is referred to the web version of this article.)

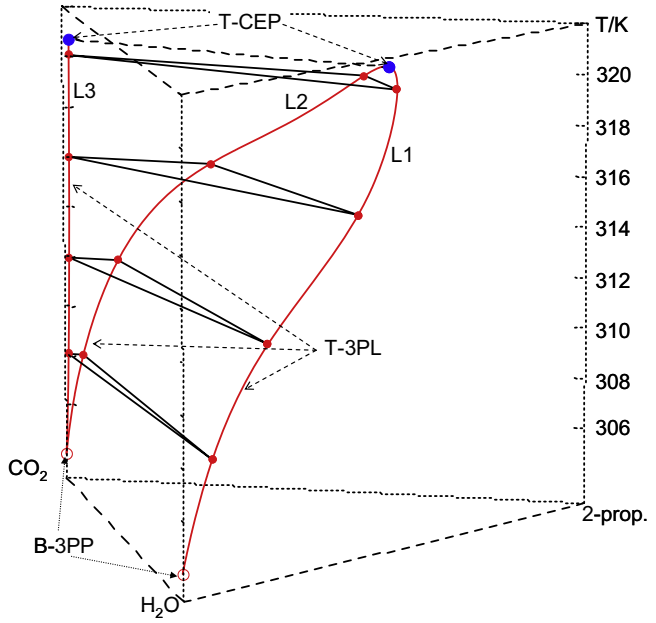


**Fig. 12.** Temperature–mole fraction projection of the same ternary three-phase line of Fig. 11. Acronyms and labels as in Fig. 11. Case 1 (Table 4). Straight solid lines: examples of calculated three-phase equilibrium tie-lines. Red solid curves: calculated phase compositions. (For interpretation of the references to color in this figure legend, the reader is referred to the web version of this article.)

at a T-CEP of higher temperature than that of the T-CEP in Figs. 11 and 12.

It is important to notice that in this work all values set for the interaction parameters are less than +1. This implies that both, $a_{ijk}$ (Eq. (2)) and $b_{ijk}$ (Eq. (5)) are positive, and therefore the mixture parameters "$a$" and "$b$" remain positive regardless the composition of the ternary (or binary) system.

The parametric study considered in this section provides evidence of the fact that by resorting to three-index ternary interaction parameters it is possible to have control on the extent of the calculated T-CELs, which in turn influence the ranges of conditions of existence of calculated three-phase equilibria. Indeed, changes in ternary interaction parameters should change all ternary phase equilibrium objects including, e.g., critical hyper

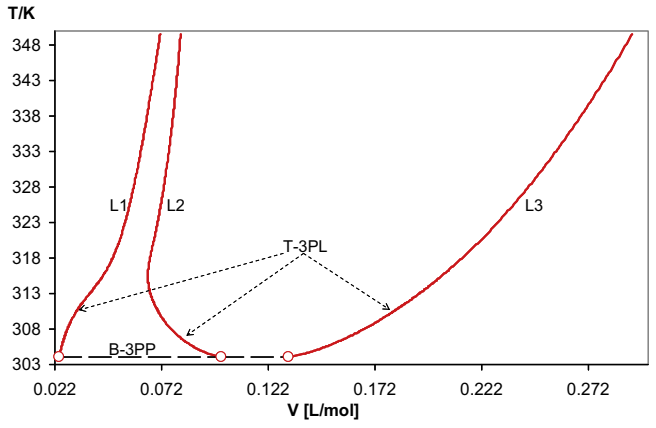


**Fig. 13.** Temperature–molar volume projection of a ternary three-phase equilibrium line calculated for the $CO_2 + H_2O$ + 2-propanol system at $P = 73$ bar, using the SRK-EOS coupled to CMRs (parameters reported in Tables 2–4). Case 2 (Table 4). Acronyms: B-3PP: binary three phase point (empty circles); T-3PL: ternary three phase line. The L1, L2 and L3 labels identify each phase in equilibrium. L3 is a vapor phase.

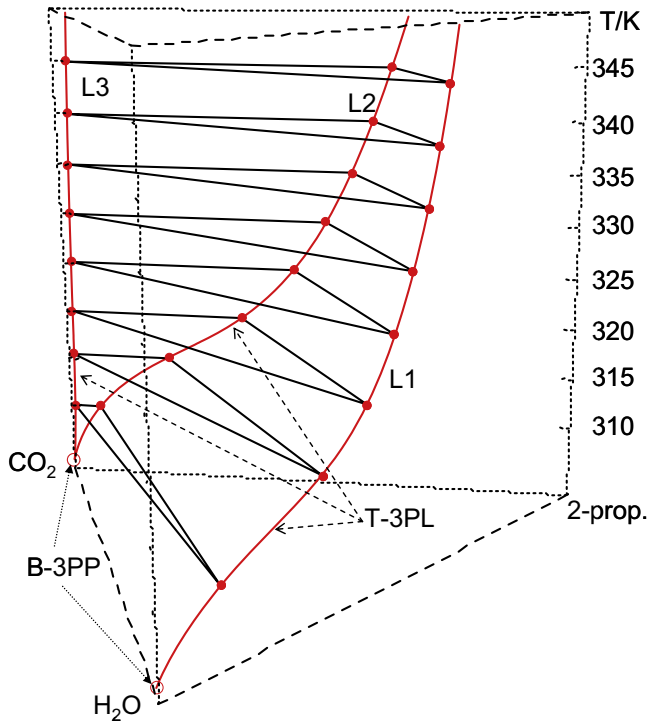


**Fig. 14.** Temperature–mole fraction projection of the same ternary three-phase line of Fig. 13. Case 2 (Table 4). Acronyms and labels as in Fig. 13. Straight solid lines: examples of calculated three-phase equilibrium tie-lines. Red solid curves: calculated phase compositions. (For interpretation of the references to color in this figure legend, the reader is referred to the web version of this article.)

surfaces, azeotropic hyper-lines and T-4P lines (with calculated phase behavior of binary subsystems indifferent to changes in ternary interaction parameters).

## 4. Remarks and conclusions

When using quadratic mixing rules (QMRs), the calculated ternary fluid phase behavior becomes determined by the (two-index) binary interaction parameters, whose values are typically obtained by matching experimental data of the binary subsystems. Such binary parameters do not in general reproduce over wide enough ranges of conditions ternary experimental data, e.g., four phase equilibria. In contrast, cubic mixing rules (CMRs) make possible to change the calculated ternary phase equilibria under conditions of invariance of the calculated phase equilibria of the binary subsystems.

In this work, we have provided evidence on the improvement that can be gained in the description of the ternary phase behavior by resorting to three-index ternary interaction parameters.

In the first part of this work (Section 3.1), we considered the case of the system $CO_2$ (1) + *n*-hexadecane (2) + 1,8-octanediol (3). We described its phase behavior using the Peng–Robinson (PR) [11] equation of state (EOS) coupled to cubic mixing rules (CMRs) [2,3,5]. This combination was able to represent the high-pressure two-phase and three-phase equilibria of the mentioned highly non-ideal asymmetric system [$CO_2$ (1) + *n*-hexadecane (2) + 1,8-octanediol (3)]. Predicted values (Table 1) for the three-index ternary parameters [2] provided an acceptable agreement with experiment. The level of agreement was increased by using three-index ternary parameters optimized so as to reproduce the available ternary experimental data. In this work, we made no attempt to automate the fitting of ternary three-index interaction parameters.

The second part of this work (Section 3.2) was a parametric study that considered the effect on ternary phase behavior of changing the values of the ternary three-index interaction parameters over wide ranges of conditions. This parametric study led to the conclusion that the values of the CMRs [2] three-index ternary interaction parameters have a strong influence on the topology of the calculated T-CELs and the associated ternary three-phase equilibria. More specifically, the ranges of conditions of existence of T-CELs change significantly when changing the ternary parameters, and so do the ranges of conditions of existence of associated ternary three-phase equilibria. It was also shown that CMRs can induce the appearance of ternary four-phase equilibria by modifying the values of the three-index ternary interaction parameters (this takes place without changing the binary equilibria), as it happened when going from "case 1" (Table 4 and Fig. 7b) to case "case 3" (Table 4 and Fig. 9b). In "case 3", the appearance of a ternary critical end point of a four-phase line (T-CEP-4PL) was indicative of the existence of a ternary four phase equilibrium line (T-4PL). In "case 2" (Table 4) T-4PLs do not exist within the ranges of conditions considered. It is worth to emphasize that the model gives for the cases 1–3 an identical phase behavior for the three binary subsystems. This is indicative of the flexibility of the CMRs, which is also significant for binary systems, as shown in Refs. [3] and [5]. It was also illustrated through cases 1 and 2 that changes in the three-index ternary interaction parameters can be used to modify the ternary three-phase equilibria, as shown in Figs. 11–14. This can be exploited for matching experimental ternary phase equilibria.

## Acknowledgements

We are grateful to Consejo Nacional de Investigaciones Científicas y Técnicas de la República Argentina (CONICET), Universidad Nacional del Sur (U.N.S., Arg.), Universidad Nacional de Córdoba (U.N.C., Arg.) and Agencia Nacional de Promoción Científica y Tecnológica (ANPCyT, Arg.) for their financial support.

## Appendix A.

*Virial coefficients associated to an equation of state*

A given equation of state (EOS) defines, for a mixture, the compressibility factor as a function of temperature, density and composition. Such function has an associated Taylor expansion in density about the point at density equal to zero (at set temperature and composition). A given term in the expansion equals the product of an integer power of density times a coefficient which depends on temperature and composition. Such coefficient is named "virial coefficient". From statistical mechanics [19], the virial coefficients are or should be multiple summations of terms having statistical weights such as $x_i x_j$ (second virial coefficient, $B$), $x_i x_j x_k$ (third virial coefficient, $C$), $x_i x_j x_k x_l$ (fourth virial coefficient, $D$) and so on, where $x_m$ is the mole fraction of component $m$. Thus, the $B$ coefficient given by the chosen EOS should be a double summation quadratic in mole fraction, the $C$ coefficient a triple summation cubic (third order) in mole fraction, etc. The van der Waals EOS (VdW) [19] and also the PR [11] and SRK [16] EOSs, have a second virial coefficient such that [$B = b - a/(RT)$], where $T$ is the absolute temperature. This means that the CMRs defined by Eqs. (1)–(6) of the main text give a $B$ coefficient which is a triple summation cubic in mole fraction, in contrast to the supposedly correct form, i.e., the quadratic double summation. This would make the CMRs "theoretically incorrect". For the case of asymmetric mixtures such as those considered in this work, Yokozeki [20] has, however, put in doubt the requirement of a

quadratic (with respect to mole fraction) second virial coefficient, associated to a given combination of equation of state and mixing rules. He concludes that for asymmetric mixtures the statistical weight cannot be "theoretically" a simple quadratic, $x_A x_B$, form. Besides, it can be shown that for the simple VdW EOS the higher virial coefficients have the expressions $[C = b^2]$, $[D = b^3]$, $[E = b^4]$, etc., where $b$ is the co-volume parameter. Thus, a linear mixing rule for $b$ ($b = b_{lin}$), gives, for the VdW–EOS, a quadratic function for $C$. Since a quadratic function is a particular case of a cubic function, the $b = b_{lin}$ choice is consistent with the supposedly theoretically correct behavior for $C$. Using similar arguments, it is concluded that the same is true, for $D$, $E$ and all higher virial coefficients of the VdW–EOS used with $b = b_{lin}$. If a quadratic mixing rule is used for $b$ ($b = b_{quad}$) in the VdW–EOS, then, the mixture third and higher virial coefficients have orders with respect to mole fractions higher than the "theoretically correct" ones. It is known, however, that $b = b_{lin}$ is a choice with significantly limited flexibility. Thus, a quadratic mixing rule is often chosen for $b$ ($b_{quad}$), which provides an extra independent interaction parameter useful to improve the reproduction of experimental information. From the previous discussion, it should be clear that the simplest EOS able to describe equilibria between fluid phases, i.e., the VdW–EOS, coupled to one of the simplest choices for the composition dependence of $b$, i.e., $b_{quad}$, already "violates" the restrictions set by statistical mechanics on the composition dependence for $C$, $D$, $E$ and higher virial coefficients. Consequently, if an EOS is to be of any practical value, "violations" to theoretical restrictions set by statistical mechanics, on virial coefficients associated to the EOS, seem to be unavoidable. Notice that the "violations" related to the virial coefficients $C$, $D$, $E$ . . . , associated to the choice $b = b_{quad}$, coexist, if $a = a_{quad}$, with the supposedly "right" form for the composition dependence of the second virial coefficient $B$, as it should be clear from the equation $[B = b - a/(RT)]$.

## Appendix B.

See Fig. B1.

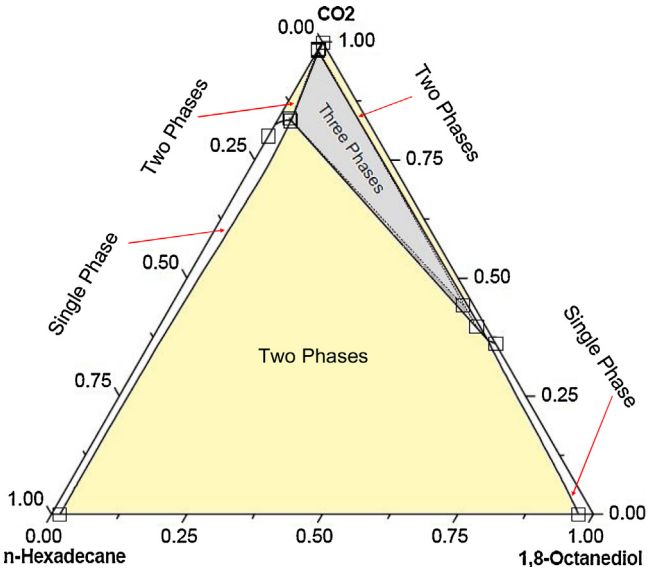


**Fig. B1.** This figure is identical to Fig. 5 of the main text except in the colouring of the equilibrium regions, carried out for a better visualization. Three yellow regions: two phases. One gray region: three phases. Three white regions: one homogeneous phase. Only two of the white regions are visible in the scale of the figure. There is another, very narrow, white region in the close vicinity of the $CO_2$ vertex. (For interpretation of the references to color in this figure legend, the reader is referred to the web version of this article.)

## Appendix C.

*Calculated binary characteristic maps related to system $CO_2$ (1) + $H_2O$ (2) + 2-propanol (3)*

In this appendix, we present the calculated characteristic maps, in their pressure–temperature projections, for the binary systems $CO_2$ (1) + $H_2O$ (2), $CO_2$ (1) + 2-propanol (3) and $H_2O$ (2) + 2-propanol (3). The model is SRK-EOS + CMRs with the binary three-index interaction parameters reported in Table 3 of the main text. Also, some calculated T-CELs are shown. The acronyms for this appendix are defined in Table C1.

Fig. C1 shows that the binary system $CO_2$ (1) + $H_2O$ (2) presents a critical line (B-CL) that originates at the pure water critical point (CP), and extends indefinitely towards high pressures; and Fig. C2

**Table C1**
Acronyms in Appendix C.

| Acronym | Meaning |
|---|---|
| B-CEP | Binary critical end point |
| B-CL | Binary critical line |
| B-CM | Binary phase behavior characteristic map |
| B-3PL | Binary three phase (equilibrium) line |
| CP | Pure compound critical point |
| P-VP | Pure compound vapor–liquid equilibrium line |

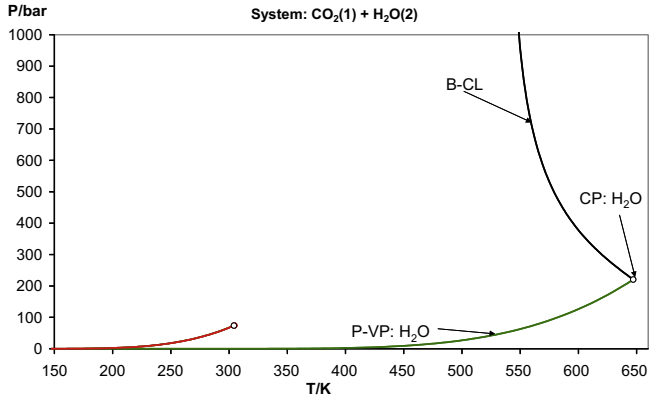


**Fig. C1.** Pressure–temperature projection of the characteristic map calculated for the $CO_2$ + $H_2O$ system using the SRK-EOS coupled to CMRs (parameters in Tables 2 and 3 of main text). Phase behavior: type III [9].

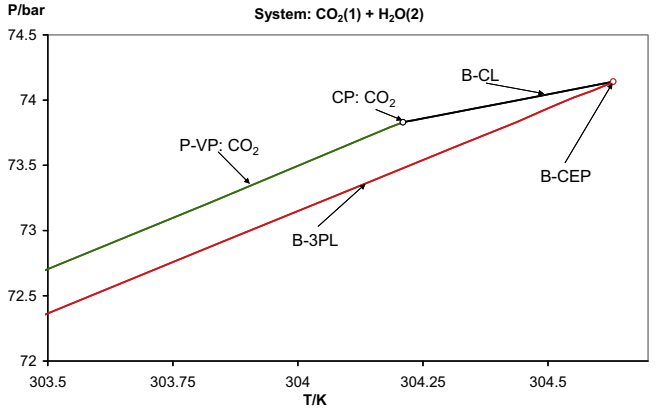


**Fig. C2.** Zoom of Fig. C1.

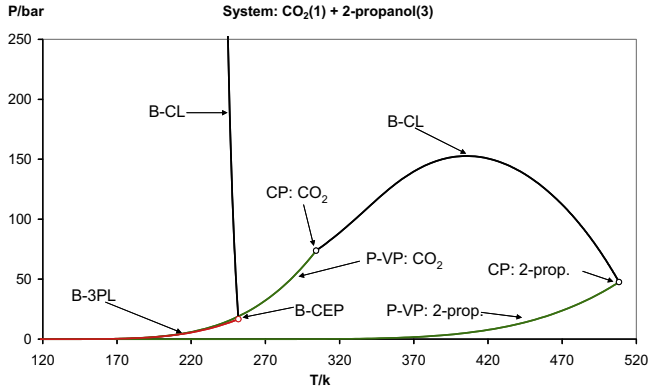


**Fig. C3.** Pressure–temperature projection of the characteristic map calculated for the $CO_2$ + 2-propanol system using the SRK-EOS coupled to CMRs (parameters in Tables 2 and 3 of main text). Phase behavior: type II [9].

shows a second critical line connecting the pure $CO_2$ (1) critical point and a binary critical end point (B-CEP) where a binary critical phase is at equilibrium with a binary non-critical phase. A binary three-phase equilibrium line (B-3PL) originates at the B-CEP and extends towards low temperatures. This is a type III [9] phase behavior, which indicates a high level of immiscibility [17] between the components of the binary system.

Fig. C3 shows that the behavior of system $CO_2$ (1) + 2-propanol (3) is of type II [9], which is characterized by the presence of a binary critical line, of the vapor–liquid type, connecting the two pure compound critical points, and also by the presence of a second critical line, which is of the liquid–liquid type, that ends at a B-CEP where a B-3PL originates. To the left of the low temperature B-CL there is liquid–liquid equilibrium in proper overall concentration ranges. Type II systems present more miscibility than type III systems.

Figs. C4 and C5show calculated T-CELs together with computed binary univariant phase equilibrium lines. Fig. C5 includes the univariant phase equilibrium lines of the binary system $H_2O$ (2) + 2-propanol (3), which indicate a type I [9] phase behavior for this binary. These behavior is characterized by the presence of a single critical line connecting both pure compound critical points. There are neither three-phase lines nor liquid–liquid critical lines in type I behavior, i.e., liquid–liquid equilibrium is not observed.

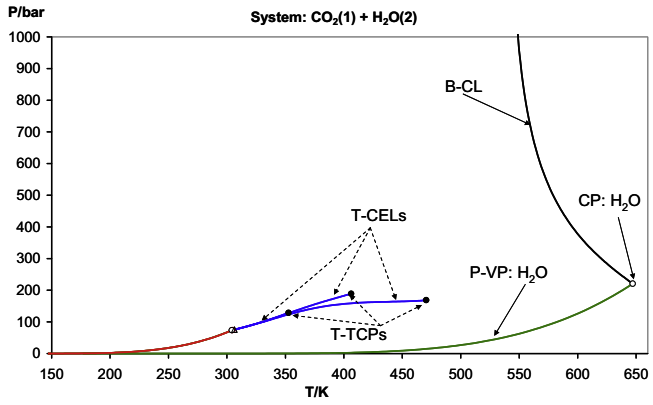


**Fig. C4.** In this figure, the curves in Fig. 6 (ternary system, main text) and in Fig. C1 are shown together. For more details see, in the main text, Figs. 6,7a and b, 8a and b and 9a and b.

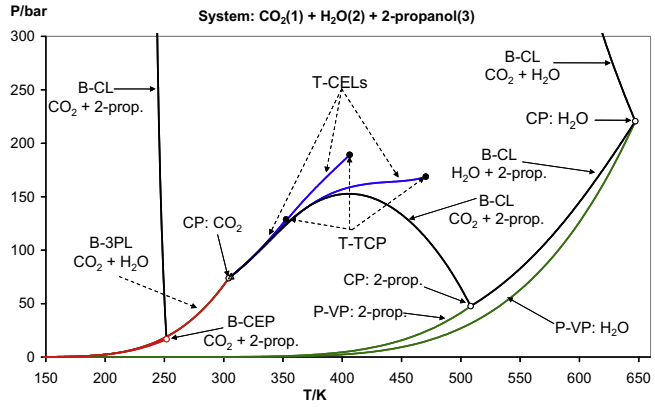


**Fig. C5.** In this figure, the curves in Figs. C1–C4 are shown together. The pressure–temperature projection of the phase behavior characteristic map, of the binary system water + 2-propanol, calculated using the SRK-EOS coupled to CMRs, with parameters reported in Tables 2 and 3, is also included. The water + 2-propanol system has a calculated type I [9] behavior. For a more detailed view at conditions including those of the critical point of pure $CO_2$ see, in the main text, Figs. 6, 7a and b, 8a and b and 9a and b.

## Appendix D.

### *Nature of tricritical points*

According to Ref. [8], in the context of binary systems, if two critical endpoints (B-CEPs) of a different nature, both located on the same three-phase curve, coincide, then, the resulting special point is named (unsymmetrical) tricritical point. The words "different nature" mean that for one of the B-CEPs the critical phase is the light one, and, for the other, the denser one. The number of degrees of freedom ($F$) of a binary tricritical point (B-TCP) equals minus one ($-1$). When using a thermodynamic model, the $F$ of a B-TCP can be made equal to zero by freeing a parameter, e.g., an interaction parameter. By making such parameter to vary within a suitable range, a B-TCP can be captured and computed. Such process would define a couple of binary critical end-lines (not observable in the laboratory) of different nature, both existing in a space which includes the free parameter as one of its variables, and both meeting at the B-TCP. The process would also define a binary three-phase surface and a couple of binary critical surfaces. In the context of ternary systems, if two T-CELs of a different nature, being both of them boundaries of the same ternary three-phase surface, coincide at point in the multi-dimensional space, then, such T-TCP point should be considered to be of the unsymmetrical type, since the described behavior is analogous to that of an unsymmetrical B-TCP. For ternary systems, an example of an unsymmetrical T-TCP is the one shown in Fig. B-5 of Ref. [7]. It seems to us that all T-TCPs calculated in this work are of the unsymmetrical type. This would be verified by carrying out additional T-CEL computations.

## References

[1] T. Adrian, M. Wendland, H. Hasse, G. Maurer, J. Supercrit. Fluids 12 (1998) 185–221.
[2] M.S. Zabaloy, Ind. Eng. Chem. Res. 47 (2008) 5063–5079.
[3] M. Cismondi, J.M. Mollerup, M.S. Zabaloy, J. Supercrit. Fluids 55 (2010) 671–681.
[4] M. Cismondi, J. Mollerup, Fluid Phase Equilib. 232 (2005) 74–89.
[5] M. Cismondi, S.B. Rodríguez-Reartes, J.M. Milanesio, M.S. Zabaloy, Ind. Eng. Chem. Res. 51 (2012) 6232–6250.
[6] G. Pisoni, M. Cismondi, L. Cardozo-Filho, M.S. Zabaloy, Fluid Phase Equilib. 362 (2014) 213–226.
[7] G. Pisoni, M. Cismondi, L. Cardozo-Filho, M.S. Zabaloy, J. Supercrit. Fluids 89 (2014) 33–47.

[8] A. Bolz, U.K. Deiters, C.J. Peters, T.W. de Loos, Nomenclature for phase diagrams with particular reference to vapour–liquid and liquid–liquid equilibria (technical report), Pure Appl. Chem. 70 (1998) 2233–2257.
[9] R.L. Scott, P.H. Van Konynenburg, Discuss. Faraday Soc. 49 (1970) 87–97.
[10] M. Spee, G.M. Schneider, Fluid Phase Equilib. 65 (1991) 263–274.
[11] D.-Y. Peng, D.B. Robinson, Ind. Eng. Chem. Fundam. 15 (1976) 59–64.
[12] M.S. Zabaloy, J.H. Vera, Fluid Phase Equilib. 119 (1996) 27–49.
[13] M.L. Michelsen, H. Kistenmacher, Fluid Phase Equilib. 58 (1990) 229–230.
[14] J. Schwartzentruber, H. Renon, Fluid Phase Equilib. 67 (1991) 99–110.
[15] J.R. Di Andreth, Multiphase behavior in ternary fluid mixture, Ph.D. Thesis, Deparment of Chemical Engineering, University of Delaware, Delaware, USA, 1985, pp. 164.
[16] G. Soave, Chem. Eng. Sci. 27 (1972) 1197–1203.
[17] J.M. Milanesio, M. Cismondi, L. Cardozo-Filho, L.M. Quinzani, M.S. Zabaloy, Ind. Eng. Chem. Res. 49 (2010) 2943–2956.
[18] M. Cismondi, M.L. Michelsen, J. Supercrit. Fluids 39 (2007) 287–295.
[19] J.P. O'Connell, J.M. Haile, Thermodynamics Fundamentals for Applications, Cambridge University Press, Cambridge, 2011 pp. 157, 166.
[20] A. Yokozeki, Int. J. Thermophys. 22 (2001) 1057–1071.
[21] R.L. Rowley, W.V. Wilding, J.L. Oscarson, Y. Yang, N.A. Zundel, T.E. Daubert, R.P. Danner, DIPPR Data Compilation of Pure Compound Properties, AIChE, Design Institute for Physical Properties, New York, 2003.